 doi:10.20944/preprints202201.0056.v1

Electrospun $ZnSnO_3$/ZnO composite nanofibers and its air-sensitive properties

Songao Dong[a,b*], Xiaoyun Jin[b], Junlin Wei[b], Hongyan Wu[a*]

[a] Institute of Advanced Materials and Flexible Electronics (IAMFE), School of Chemistry and Materials Science,

Nanjing University of Information Science and Technology, Nanjing 210044, China

[b] Institute of Material Science and Engineering, Jiangsu University of Science and Technology, Zhenjiang 212003,

China

Abstract

In this work, a novel heterojunction based on $ZnSnO_3$/ZnO nanofibers was prepared using electrospinning method. The crystal, structural and surface compositional properties of sample based on $ZnSnO_3$ and $ZnSnO_3$/ZnO composite nanofibers were investigated by X-ray diffractometer (XRD), Scanning electron microscope (SEM), X-ray photoelectron spectrometer (XPS) and Brunauer-Emmett-Teller (BET). Compared to pure $ZnSnO_3$ nanofibers, the $ZnSnO_3$/ZnO heterostructure nanofibers display high sensitivity and selectivity response with fast response towards ethanol gas at low operational temperature. The sensitivity response of sensor based on $ZnSnO_3$/ZnO composite nanofibers were 19.6 towards 50 ppm ethanol gas at 225°C, which was about 1.5 times superior than that of pure $ZnSnO_3$ nanofibers, which can be owed mainly to the presence of oxygen vacancies and the synergistic effect between $ZnSnO_3$ and ZnO.

Keywords: Electrospinning; $ZnSnO_3$/ZnO nanofibers; Sensing performance; n-n heterojunction

* Corresponding author.

E-mail addresses: stdong@just.edu.cn (Songtao Dong); wuhy2009@nuist.edu.cn (Hongyan Wu)

Preprints (www.preprints.org) | NOT PEER-REVIEWED | Posted: 6 January 2022 doi:10.20944/preprints202201.0056.v1

1. Introduction

In recent years, with the increasing demand for the detection of toxic gases, volatile organic compounds and clinical gas analysis, gas sensor research has become more and more extensive. High sensitivity, fast response, excellent selectivity and long-term stability are the basic parameters of a highly sensitive gas sensor [1]. Semiconductor metal oxide gas sensors have attracted much attention because of their advantages such as fast response, low cost, simple structure and good compatibility. Semiconductor metal oxide materials(e.g. NiO [2], SnO_2 [3,4], ZnO [5], CuO [6], etc.) are widely used for their high performance, cost effectiveness and excellent gas sensing properties, but these binary oxide materials operate at high temperatures, so the search for a sensing material with low operating temperature and high sensitivity has become the focus of current research.

At present, ternary transition metal oxides as new gas-sensitive materials have received widespread attention due to their excellent gas-sensitive properties, structural stability, especially their unique energy band structure and unique physical and chemical properties. However, due to insufficient exposure area and low electron transfer, many ternary metal oxides tend to show lower gas sensitivity [7]. Among the ternary tin-based metal oxides, $ZnSnO_3$ is a typical perovskite structure oxide material with Zn at the A-site and Sn at the B-site. Compared to ZnO and SnO_2, $ZnSnO_3$ has been widely used in gas sensors for its high chemical sensitivity and excellent electrical properties [8]. The spatial arrangement of the atoms in the $ZnSnO_3$ system is an octahedron. The special crystal structure of $ZnSnO_3$ can have a lot of oxygen vacancies, provide more oxygen adsorption sites, can promote the reaction with reducing gases, thereby improving the gas sensitivity [8]. Many studies have focused on single component $ZnSnO_3$ as a gas sensing material. Wang et al.[9] reported that the sensitivity response to 100 ppm H_2S of hollow, cubic-structured $ZnSnO_3$ sample was up to 1418 at an optimum operating temperature of 335℃. $ZnSnO_3$ nanomicrospheres was prepared by hydrothermal method, which had high selectivity for n-butanol at 200°C [10]. Wang and his team found that $ZnSnO_3$ samples prepared by co-precipitation and heat treatment had a high sensitivity response to ethanol, reaching 147 [11]. Researchers have also prepared heterogeneous structures to improve gas sensing performance, such as $ZnSnO_3/TiO_2$, SnO_2/TiO_2, WO_3/SnO_2 and $ZnSnO_3$/ZnO [12-15]. To further improve the gas-sensitive performance of $ZnSnO_3$, Yu et al.compounded $ZnSnO_3$ with CuO and found a sensitivity response to ethanol of up to 131 [16] . Zhang et al.[17] and Cheng et al.[18] reported that $ZnSnO_3$ was compounded with SnO_2, respectively, due to the excellent physical and chemical properties of both SnO_2 and $ZnSnO_3$, the gas-sensitive properties of the $SnO_2/ZnSnO_3$ composite were significantly improved compared to both SnO_2 and $ZnSnO_3$ materials. The cubic $ZnSnO_3$/ZnO heterostructure showed a much improved response to 50 ppm triethylamine compared to pure $ZnSnO_3$ (R_a/R_g=21) [15]. These results indicate that heterostructures composed of MO_x and $ZnSnO_3$ have great potential for gas sensing applications.

Currently, researchers can prepare $ZnSnO_3$ nanofibers with different morphologies (e.g. spherical, polyhedral, etc.)[19,20], but there are few reports on nanofiber samples with $ZnSnO_3$-based heterojunctions. The electrospinning method allows to obtain nanofibrous materials with high specific surface area and different morphologies. Based on the above considerations, $ZnSnO_3$ nanofibers and $ZnSnO_3$/ZnO composite nanofibers were synthesised by electrospinning in this paper. The results of gas-sensitive performance of $ZnSnO_3$ nanofibers and $ZnSnO_3$/ZnO nanofibers showed that the $ZnSnO_3$/ZnO nanofibers had a lower operating temperature (225℃), a sensitivity response of 19.6 at 50 ppm in ethanol atmosphere and better stability than $ZnSnO_3$. The possible enhanced gas sensing mechanism was proposed.

2 Experimental section

2.1 Material preparation

A combination of electrospinning and calcination was used to prepare $ZnSnO_3$/ZnO

Preprints (www.preprints.org) | NOT PEER-REVIEWED | Posted: 6 January 2022 doi:10.20944/preprints202201.0056.v1

nanofibers. The experimental procedure was as follows: First, appropriate amounts of stannous chloride ($SnCl_2 \cdot 2H_2O$) and zinc chloride ($ZnCl_2$) were dissolved in a mixed solution of 8 g N, N-dimethylformamide (DMF) and 12 g anhydrous ethanol under constant stirring so that the molar ratio of Sn^{4+} to Zn^{2+} was 1:1.2. Next, 2 g of PVP (average molecular weight of 1300000 g mol^{-1}) was added and stirred thoroughly to finally obtain the precursor solution required for the electrospinning method. The electrospinning precursor solution was then loaded into a plastic syringe with a 22-gauge needle and the advance rate of the syringe pump was set at 0.4 mL h^{-1}. A voltage of 15 kV is applied between the needle and the collector, and a layer of aluminium foil is wrapped around the rotating receiver 20 cm from the needle to collect the fibres. The collected precursor fibers were calcined in air at 450 °C for 2 h to obtain $ZnSnO_3$/ZnO nanofibers.

2.2 Characterization

The physical phases of the calcined samples were analysed by X-ray powder diffractometer (XRD, Bruker D8 Advance) using a copper target K_α line with a scanning range of 20 - 60° and a scanning speed of 6°/min. The field emission scanning electron microscopy (Merlin Compact, Carl Zeiss, Germany) was used to characterize morphology of the samples. Thermogravimetric tests were carried out by a thermal analysis system (Diamond TG/DTA, Perkin Elmer S. A.) to determine the calcination temperature of the precursors, using samples weighing 4 - 6 mg and heated to 600 °C at a heating rate of 15 °C/min. The elemental composition and valence states in the material were characterized using an X-ray photoelectron spectrometer (Thermo Scientific K-Alpha, XPS). Specific surface area of the prepared nanofibers by N_2 adsorption/desorption test (BET, Micromeritics ASAP 2020).

2.3 Gas-sensitive performance measurement

A 200 mg sample of $ZnSnO_3$/ZnO nanofibers was mixed well with 0.2 mL of deionised water in an agate mortar and ground to a paste. The ground paste sample is then uniformly coated on the surface of the Ag-Pd forked finger electrode on an Al_2O_3 substrate and dried for a certain period of time to obtain the gas sensitive element required for the test. Before testing, the dried gas-sensitive elements are aged in air for 10 h. The sensitivity response, operating temperature and stability of the preparations were tested on the CGS-1TP Intelligent Gas Sensitive Analysis System.

3 Results and Discussion

3.1 Microstructure and morphology

In order to determine the calcination temperature of the $ZnSnO_3$ precursor obtained by electrospinning methods, TG tests were carried out on the $ZnSnO_3$ precursor in an air atmosphere in the temperature range of 30 - 600 °C with a heating rate of 15 °C/min. The results are shown in Figure 1(a). The graph shows an 8 wt% drop in sample mass at 300 ℃. This is due to the evaporation of organic solvents and the evaporation of gases and moisture adsorbed on the surface of the sample. The sharp decrease in sample mass around 350 ℃ can be attributed to the decomposition of the precursor, while the significant drop in the curve around 400℃ can be attributed to the decomposition of PVP. In addition, no significant weight changes were observed above 450 ℃, which proves that all organic matter in the precursor decomposes at 450 ℃ and that calcination of the precursor at temperatures higher than 450 ℃ is sufficient. Figure 1(b) shows the XRD results of the $ZnSnO_3$/ZnO precursor after 2 h of calcination at 450 ℃. A comparison with the standard card (PDF No. 28-1486) shows that the XRD diffraction peaks at 2θ of 26.5°, 33.7°, 37.7°, 51.6° and 54.6° correspond to the (012), (110), (015), (116), (018) and (214) crystal planes of $ZnSnO_3$, respectively. The remaining XRD diffraction peaks were compared with the standard card (PDF No. 65-3411) and were found to correspond to (100), (101), (102) and (110) crystal planes at 2θ of 31.7°, 36.3°, 47.5° and 56.6°, respectively. That is, the XRD diffraction peak corresponding to the standard card (PDF No. 65-3411) is the diffraction peak of ZnO. The results show that the $ZnSnO_3$/ZnO

Preprints (www.preprints.org) | NOT PEER-REVIEWED | Posted: 6 January 2022 doi:10.20944/preprints202201.0056.v1

precursors were successfully prepared after calcination in air at 450 ℃ for 2 h.

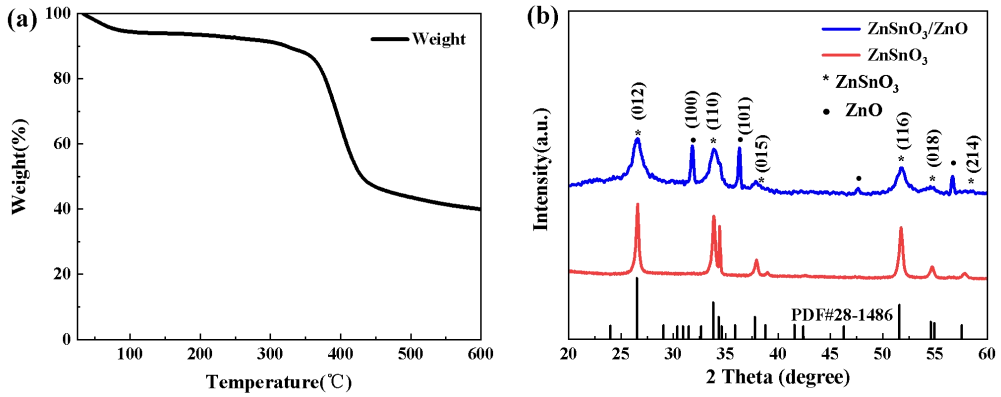

Figure 1 (a) TG test results of $ZnSnO_3$ precursors; (b) XRD of $ZnSnO_3$ and $ZnSnO_3$/ZnO calcined at 450 °C

Figure 2(a) and (b) shows the SEM results of $ZnSnO_3$ samples prepared after calcination at 450 ℃ for 2 h in an air atmosphere. As can be seen in Figure 2(a), the $ZnSnO_3$ sample after calcination at 450 ℃ for 2 h in an air atmosphere is coarse and uniformly fibrous, with no breakage of the continuous fibers. The average diameter of the $ZnSnO_3$ sample is about 300 - 400 nm, as shown in Figure 2 (b). Figure 2(c) and (d) shows the SEM results of $ZnSnO_3$/ZnO samples prepared after calcination at 450 ℃ for 2 h in air atmosphere. As can be seen in Figure 2(c), the $ZnSnO_3$/ZnO sample exhibits uniformly coarse and fine fibers with no fracture in the fiber continuity. The average diameter of the $ZnSnO_3$/ZnO nanofibers is even smaller, around 200 nm, as shown in Figure 2(d). Due to the low calcination temperature of 450 ℃, the rate of gas production from the decomposition of pharmaceuticals is slow and the pressure difference between the interior and exterior of the fibers is not large, so no hollow structure is formed [21]. The above experiments show that the diameter of the $ZnSnO_3$/ZnO nanofibers obtained by compounding $ZnSnO_3$ with ZnO is significantly reduced compared to the $ZnSnO_3$ nanofibre samples.The BET analysis shows that the specifc surface area of the $ZnSnO_3$/ZnO nanofibers (31.24 m^2 g^{-1}) was substantially larger than that of pristine $ZnSnO_3$ nanofibers (20.15 m^2 g^{-1}).

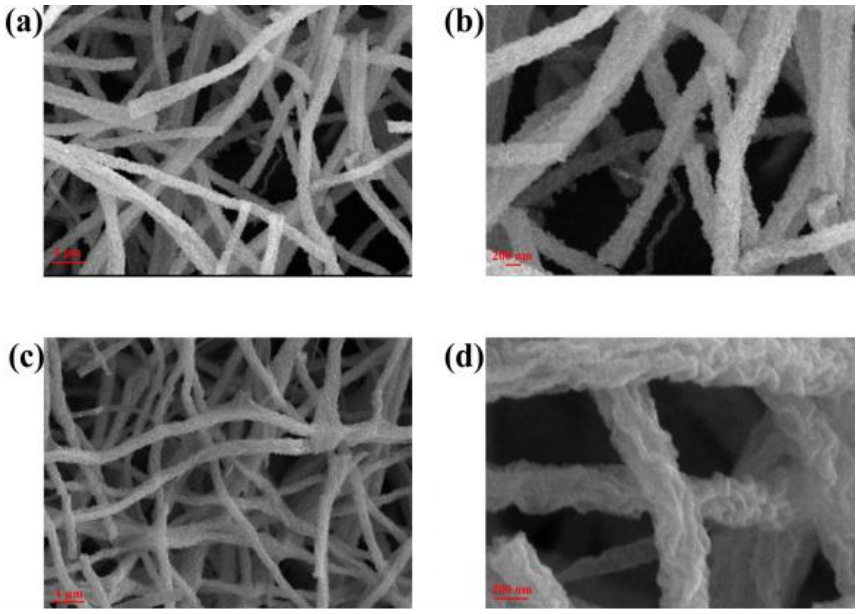

Figure 2 SEM images of $ZnSnO_3$ and $ZnSnO_3$/ZnO: (a) and (b) $ZnSnO_3$; (c) and (d) $ZnSnO_3$/ZnO

XPS are carried out to study the elemental composition and valence states in

Preprints (www.preprints.org) | NOT PEER-REVIEWED | Posted: 6 January 2022 doi:10.20944/preprints202201.0056.v1

$ZnSnO_3$/ZnO, and the results are shown in Figure 3. Figure 3 (a) shows the full XPS spectrum of the $ZnSnO_3$/ZnO nanofibers, from which it can be observed that the obtained $ZnSnO_3$/ZnO nanofibers contain the elements Zn, Sn, C and O. The peak at 284.8 eV corresponds to the spin-orbit peak of C 1s.The broad XPS spectrums of the Zn-2p range, Sn-3d and O-1s range are shown in Fig.3(b) and (d). In case of Zn-2p spectrum, the Zn-2p peak can be distributed into two signals as shown in Fig. 3(b). Zn-$2p_{3/2}$ and Zn-$2p_{1/2}$ signals are focused at 1021.1 eV and 1044.1eV, respectively, which indicates that the chemical valence of Zn in the system is +2 [22]. As shown in Fig. 3(c), the two peaks at 486.8 and 495.1 eV correspond to the Sn $3d_{5/2}$ and Sn $3d_{3/2}$ spin-orbit peaks, respectively. The bimodal spin orbit shows a split value of approximately 8.3 eV, indicating the presence of Sn^{4+} cations [23]. The O_{1s} spectrum of $ZnSnO_3$ and $ZnSnO_3$/ZnO is illustrated in Fig. 3(d) and (e), which is deconvolved into three characteristic peaks by Gaussian fitting[16,24]. The three fitting peaks are attributed to three important oxygen species [25], denoted as O_L, O_V, O_C, respectively, corresponding to O^{2-} species in the crystal lattice, VOs and chemically adsorbed or dissociated oxygen species, respectively [26]. The three characteristic peaks of O1s in $ZnSnO_3$ nanofibers are located at 530.06 eV, 531.65 eV and 533.13 eV, while the characteristic peaks of O1s in $ZnSnO_3$/ZnO nanofibers are located at 529.99 eV, 531.33 eV, and 532.27 eV, which can be corresponded to the O_L, O_V, O_C species, respectively[17,27]. It must be pointed out that the gas sensitivity characteristics may be highly dependent on the type of VO present on the semiconductor surface [28]. Fig. 4(f) shows that the relative percentage of each oxygen species in $ZnSnO_3$ and $ZnSnO_3$/ZnO nanofibers. The proportion of oxygen species in obtained $ZnSnO_3$ and $ZnSnO_3$/ZnO nanofibers are shown in the table 1. The results of Fig.4(f) and table 1 are clear that compared with the percentage of Ov of $ZnSnO_3$ nanofibers, that of $ZnSnO_3$/ZnO nanofibers substantially increases.

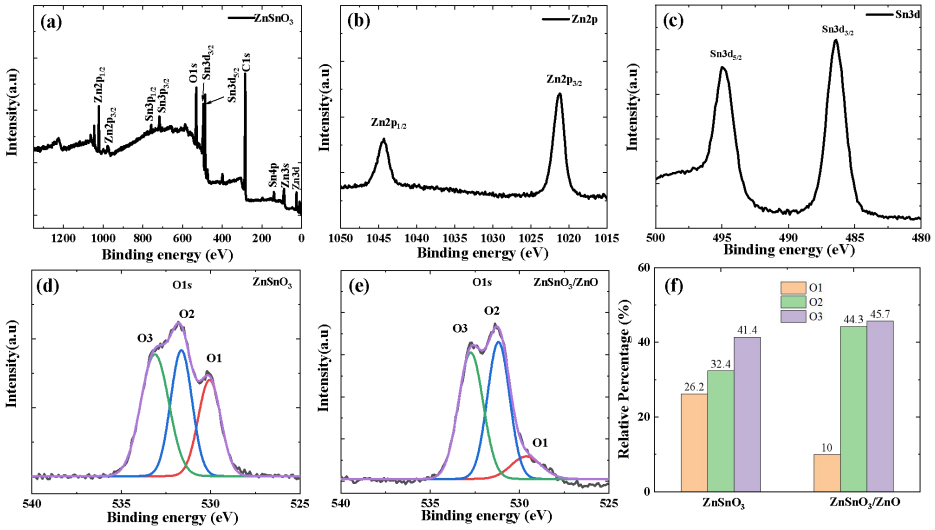

Fig.3 XPS spectra of $ZnSnO_3$/ZnO nanofibers: (a) a survey spectrum, high resolution spectra for (b) Zn 2p, (c) Sn3d, (d) O1s (of $ZnSnO_3$),(e) O1s (of $ZnSnO_3$/ZnO), (f) fitting results of O 1s XPS spectra of $ZnSnO_3$ and ZnO/$ZnSnO_3$.

Table 1 The proportion of oxygen species in obtained $ZnSnO_3$ and ZnO/$ZnSnO_3$ nanofibers.

Sample	O^{2-}(%)	O^{-}(%)	O_2-(%)
$ZnSnO_3$	26.2%	32.4%	41.4%
ZnO/$ZnSnO_3$	10%	44.3%	45.7%

Preprints (www.preprints.org) | NOT PEER-REVIEWED | Posted: 6 January 2022 doi:10.20944/preprints202201.0056.v1

3.2 Gas-sensitive properties of $ZnSnO_3$/ZnO nanofibers

It is well known that changes in operating temperature can highly influence the gas sensing characteristics of sensing materials. To verify this, the response of $ZnSnO_3$ samples and $ZnSnO_3$/ZnO composite nanofibers toward 50 ppm ethanol gas are tested at different temperatures and the results are shown in Figure 4. Figure 4(a) show that the response of the $ZnSnO_3$ sample increases with increasing temperature untill the temperature rises to 300 °C, when the response is maximum at 13.4. Then the temperature continues to increase and the response decreases instead. Figure 4(b) shows the sensitivity response of $ZnSnO_3$/ZnO samples towards 50 ppm ethanol gas at different temperatures. From the graph it can be concluded that the optimum working temperature for the $ZnSnO_3$/ZnO sample is 225°C and the sensitivity response for the $ZnSnO_3$/ZnO sample is 19.6. The optimum operating temperature of the $ZnSnO_3$/ZnO sample is significantly lower than that of the $ZnSnO_3$ sample. The sensitivity response has also been improved, with a 46.3 % increase in sensitivity response.

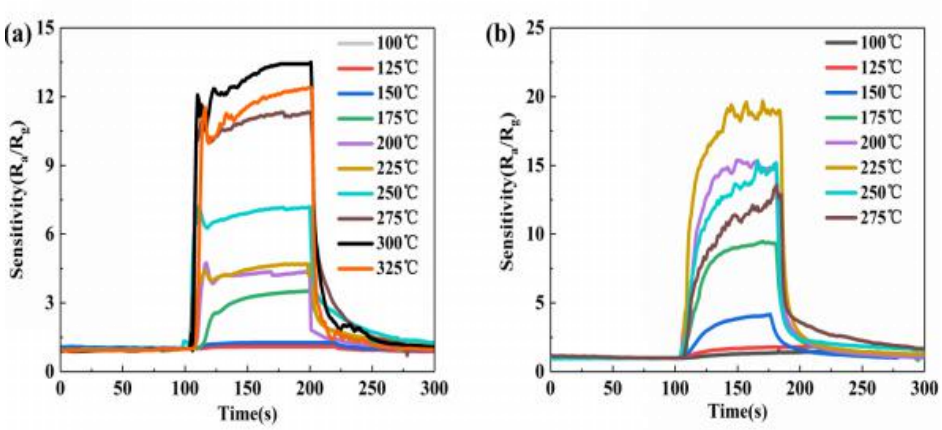

Fig.4 Sensitivity of $ZnSnO_3$ and $ZnSnO_3$/ZnO towards 50 ppm ethanol at different temperatures: (a) $ZnSnO_3$; (b) $ZnSnO_3$/ZnO

To further investigate the gas-sensitive performance of the $ZnSnO_3$/ZnO samples, the response of $ZnSnO_3$ and $ZnSnO_3$/ZnO samples to different concentrations of ethanol and the stability of the response to 50 ppm ethanol were tested at the optimum operating temperature, respectively, and the results are shown in Figure 5. As seen in Fig. 5(a), the response of $ZnSnO_3$/ZnO increases with increasing ethanol concentration due to the fact that with increasing ethanol concentration， more ethanol molecules react with the oxygen ions adsorbed on the surface of the material, resulting in a higher carrier concentration and thus a subsequent increase in the response of the material. Figure 5(b) show that the response of the $ZnSnO_3$/ZnO composite samples increased with increasing ethanol concentration, while the response of the $ZnSnO_3$/ZnO samples was higher than that of the $ZnSnO_3$ samples at the same concentration of ethanol. Figure 5 (c) and (d) show the stability of the $ZnSnO_3$ sample and the $ZnSnO_3$/ZnO sample under ethanol atmosphere at 50 ppm, respectively. As can be seen from the graphs, the $ZnSnO_3$ and $ZnSnO_3$/ZnO samples showed no significant fluctuations in response after six repeated exposures to ethanol at 50 ppm, indicating that both the $ZnSnO_3$ and $ZnSnO_3$/ZnO samples have good stability. The above experimental results show that the $ZnSnO_3$/ZnO sample has a lower working temperature, higher response and better stability for ethanol atmosphere than the $ZnSnO_3$ sample.

Preprints (www.preprints.org) | NOT PEER-REVIEWED | Posted: 6 January 2022 doi:10.20944/preprints202201.0056.v1

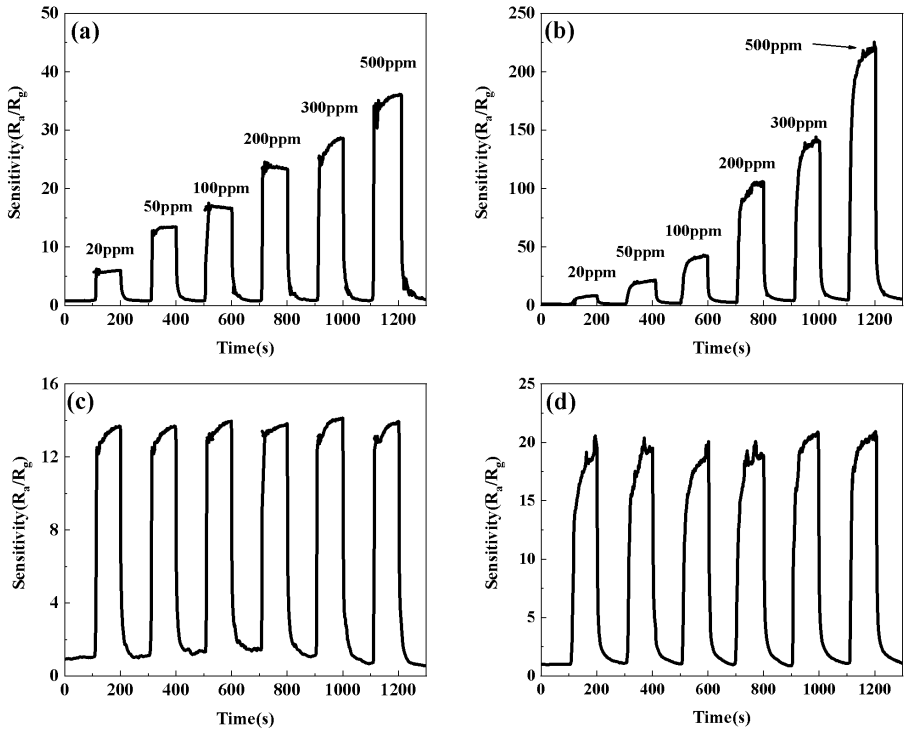

Fig.5 Sensitivity of $ZnSnO_3$ and $ZnSnO_3$/ZnO to different concentrations of ethanol at the optimal working temperature: (a) $ZnSnO_3$; (b) $ZnSnO_3$/ZnO; the best Stability of sensitivity to 50 ppm ethanol at working temperature: (c) $ZnSnO_3$; (d) $ZnSnO_3$/ZnO

3.3 Gas-sensing mechanism

The sensing mechanism based on metal oxide semiconductor gas sensor is the changed resistance caused by the adsorption and desorption of the target gas molecules on the surface of sensitive materials, which depends mainly on the concentration and mobility of the charge. Therefore, the gas-sensitive mechanism of $ZnSnO_3$ and $ZnSnO_3$/ZnO composite nanofibers can be understood simply as a surface-controlled mechanism. The change in resistance depends on the type and amount of oxygen chemisorbed on the surface. In ambient air, the resistance of $ZnSnO_3$ and $ZnSnO_3$/ZnO composite nanofibers is mainly controlled by the concentration of adsorbed oxygen (O^- and O^{2-}). The variation in response for $ZnSnO_3$ nanofibers is mainly related to the adsorption-desorption reaction of ethanol gas on the surface of $ZnSnO_3$ samples. $ZnSnO_3$ is a typical N-type semiconductor material, when it is in the air oxygen molecules adsorbed on the surface of $ZnSnO_3$ and gain electrons and thus convert into oxygen ions. When a certain amount of oxygen ions accumulated on the material surface reaches equilibrium, an electron depletion layer is formed on the material surface, which reduces the carrier concentration of the material system and in turn leads to an increase in the material resistance. However, when $ZnSnO_3$ is placed in an ethanol atmosphere, the ethanol molecules will react with oxygen ions, releasing a large number of electrons and causing the resistance of the material to drop, the equation for the above process reaction is as follows[29]:

$$O_2(gas) \leftrightarrow O_2(ads) \qquad O_2 + e^- \rightarrow O^-, O_2^-, O^{2-} \qquad (1)$$

$$C_2H_5OH + 6O^{2-}(ads) \leftrightarrow 2CO_2 + 3H_2O + 12e^- \qquad (2)$$

According to ref [15], since both $ZnSnO_3$ and ZnO are N-type semiconductor materials, when ZnO is successfully compounded with $ZnSnO_3$ to form a homotypic heterojunction (i.e. N-N junction), this N-N junction is a key factor in improving the ethanol gas sensitivity

 doi:10.20944/preprints202201.0056.v1

between $ZnSnO_3$ and ZnO. Differences in the Fermi energy levels of two connected semiconductor compounds. The transfer of electrons from higher energy states to lower energy states until equilibrium is reached at the Fermi energy level, resulting in the formation of a depletion layer in the interface region. In contrast to $ZnSnO_3$, the electrons on the $ZnSnO_3$ conduction band in the $ZnSnO_3$/ZnO sample are transferred to the ZnO conduction band to be trapped by oxygen molecules, resulting in the formation of a large number of oxygen anions. At the same time, the electron depletion layer appears near the surface of $ZnSnO_3$/ZnO, which is an important component of the gas sensing process. In the air environment, the increased height of the potential barrier of the $ZnSnO_3$/ZnO heterostructured composite makes electron transfer more difficult, which also leads to a significant increase in sensor resistance (R_a). In an ethanol environment, the reaction of ethanol molecules with oxygen ions releases electrons back into the $ZnSnO_3$/ZnO heterojunction, resulting in an increase in electron concentration. This significantly reduces the potential barrier height of $ZnSnO_3$ and ZnO, significantly reducing the sensor resistance (R_g). The analysis of the above gas-sensitive properties revealed that the heterogeneous structure of the $ZnSnO_3$/ZnO composites enhanced electron transport and enabled effective separation of electrons and holes compared to the $ZnSnO_3$ nanofibers material.

Compared to $ZnSnO_3$ nanofibers, $ZnSnO_3$/ZnO composite nanofibers have a larger VOs of 44.3%, almost 1.5 times that of $ZnSnO_3$ nanofibers, which is conducive to improve the sensitivity characteristics of gas-sensitive materials[30]. It is also suggested that in the "chemical sensitization" mechanism established by the spillover effect, ZnO plays an important role in activating the dissociation rate of molecular oxygen[31].

4 Conclusion

In conclusion, $ZnSnO_3$ nanofibers and $ZnSnO_3$/ZnO nanofibers were successfully prepared using a simple electrospinning method. The average diameter of the $ZnSnO_3$/ZnO composite nanofibers is approximately 200 nm. Compared to $ZnSnO_3$ nanofibers, $ZnSnO_3$/ZnO nanofibers have a lower operating temperature (225 °C), higher sensitivity (19.6) and better stability in an ethanol atmosphere, which can be owed mainly to the presence of oxygen vacancies and the synergistic effect between $ZnSnO_3$ and ZnO. The results confirmed that $ZnSnO_3$/ZnO nanofibers could have an outstanding potential candidate for ethanol detection.

Author Contributions: Conceptualizatin, Xiaoyun Jin; data curation, Junlin Wei; writing—original draft preparation, Songao Dong; writing—review and editing, Hongyan Wu. All authors have read and agreed to the published version of the manuscript.

Funding: This research received no external funding.

Institutional Review Board Statement: Not applicable.

Informed Consent Statement: Not applicable.

Data Availability Statement: The data used to support the findings of this study are available from the corresponding author upon request.

Acknowledgments: The authors acknowledge fnancial support from the National Natural Science Foundation of China (51702132). Song-Tao Dong acknowledges the open project of the National Laboratory of Solid State Microstructures at Nanjing University. Jun-Lin Wei acknowledges financial support from the Postgraduate Research & Practice Innovation Program of Jiangsu Province (Grant No. KYCX20_3132).

Conflicts of Interest: The authors declare no conflict of interest.

 doi:10.20944/preprints202201.0056.v1

References

1. J. Ma, X. Xiao, Y. Zou, Y. Ren, X. Zhou, X.Yang, X. Cheng, Y. Deng, A general and straightforward route to noble metal-decorated mesoporous transition-metal oxides with enhanced gas sensing performance, Adv. Funct. Mater. 2019, 15, e1904240.
2. M. M. Gomaa, M. H. Sayed, V. L. Patil, M. Boshta, P. S. Patil. Gas sensing performance of sprayed NiO thin films toward NO_2 gas, J. Alloys Compd. 2021, 885, 160908.
3. Y. Z. Wang,Y. Zeng, L. O. Wang, Z. Lou, L. Qiao, H. W. Tian, W. T. Zheng, Ultrathin nanorod-assembled SnO_2 hollow cubes for high sensitive n-butanol detection, Sensor. Actuat. B-Chem. 2019, 283, 693-704.
4. X. Y. Kou, N. Xie, F. Chen, T. S. Wang, L. L. Guo, C. Wang, Q. J. Wang, J. Ma, Y. F. Sun. H, Zhang, G, Y, Lu. Superior acetone gas sensor based on electrospun SnO_2 nanofibers by Rh doping, Sensor. Actuat. B-Chem. 2018, 25, 6861-869.
5. J. H. Kim, A. Mirzaei, H. W. Kim, S. S. Kim, Low voltage driven sensors based on ZnO nanowires for room temperature detection of NO_2 and CO gases, ACS Appl. Mater. Interfaces 2019,11(27), 24172–24183.
6. Wangchang Geng, Zhiyan Ma, Jianhua Yang, Libing Duan, Feng Li, Qiuyu Zhang. Pore size dependent acetic acid gas sensing performance of mesoporous CuO, Sensor. Actuat. B-Chem. 2021,334, 129639.
7. K. Jain. R. P, Pant. S.T. Lakshmi-kumar, Effect of Ni doping on thick film SnO_2 gas sensor, Sensor. Actuat. B-Chem. 2006, 113, 823-829.
8. Y. Yin,Y. Shen, P. Zhou, R. Lu, A. Li, S. Zhao,W. Liu, D. Wei, K.Wei, Fabrication characterization and n-propanol sensing properties of perovskite-type $ZnSnO_3$ nanospheres based gas sensor, Appl. Surf. Sci. 2020, 509, 145335.
9. Z. Y. Wang, J. Y. Miao, H. X. Zhang, D. Wang, J. B. Sun. Hollow cubic $ZnSnO_3$ with abundant oxygen vacancies for H_2S gas sensing. J. Hazard. Mater., 2020, 391: 122226.
10. G. Q. Feng, Y. H. Che, C. W. Song, J. K. Xiao, X. F. Fan, S. Sun, G. H. Huang, Y. C. Ma Morphology-controlled synthesis of $ZnSnO_3$ hollow spheres and their n-butanol gas-sensing performance. Ceram. Int., 2021, 47: 2471-2482.
11. X. Y. Wang, X. T. Zhu, T. Tao, B. X. Leng, W. Xu, L. H. Mao, Structural inheritance and change from $ZnSn(OH)_6$ to $ZnSnO_3$ compounds used for ethanol sensors: Effects of oxygen vacancies, temperature and UV on gas-sensing properties. J. Alloys Compd. 2020, 829: 154445.
12. X.Wang,Y. Liu, B. Ding, H. Li, X. Zhu, M. Xia, Influence of the addition of nano-TiO_2 and ZnO on the sensing performance of micro-$ZnSnO_3$ ethanol sensors under UV illumination, Sensor. Actuat. B-Chem. 2018, 276, 211-221.
13. H. T. Xun, Z. B. Zhang, A. H. Yu, J. X. Yi, Remarkably enhanced hydrogen sensing of highly-ordered SnO_2 decorated TiO_2 nanotubes, Sensor. Actuat. B-Chem. 2018, 273, 983-990.
14. S. F. Shao, X. Chen,Y. Y. Chen, M. Lai, L. S. Che, Ultrasensitive and highly selective detection of acetone based on Au@WO_3-SnO_2 corrugated nanofibers, Appl. Surf. Sci. 2019, 473, 902-911.
15. Y. Yan, J. Y. Liu, H. S. Zhang, D. L. Song, J. Q. Li, P. P. Yang, M. L. Zhang, J. Wang, One-pot synthesis of cubic $ZnSnO_3$/ZnO heterostructure composite and enhanced gas-sensing performance. J. Alloys. Compd. 2019, 780,193-201.
16. S. W. Yu, X. H. Jia, J. Yang, S. Z. Wang, Y. Li, H. J. Song, Highly sensitive ethanol gas sensor based on CuO/$ZnSnO_3$ heterojunction composites. Mater. Lett., 2021, 291: 129531.
17. J. T. Zhang, X. H. Jia, D. D. Lian, J. Yang, S. Z. Wang, Y. Li, H. J. Song, Enhanced selective acetone gas sensing performance by fabricating $ZnSnO_3$/SnO_2 concave microcube. Appl. Surf. Sci., 2021, 542: 148555.
18. Pengtei Cheng, Li Lv,Yinglin Wang, Bao Zhang, Yue Zhang, Yaoqiong Zhang, Zhaohui Lei, Luping Xu. SnO_2/$ZnSnO_3$ double-shelled hollow microspheres based high-performance acetone gas sensor. Sensor. Actuat. B-Chem., 2021, 332: 129212.
19. Y Chen, L Yu, Q Li, T. Wang. An evolution from 3D face-centered-cubic $ZnSnO_3$ nanocubes to 2D orthorhombic $ZnSnO_3$ nanosheets with excellent gas sensing performance. Nanotechnology, 2012, 23(41): 415501.
20. D. Zhang, Y. Q. Zhang, Y. Fan, N. Luo, J. Xu. Micro-spherical $ZnSnO_3$ material prepared

by microwave-assisted method and its ethanol sensing properties. Chinese Chem. Lett., 2020, 31(8): 2087-2090.
21. Linlin Li, Shengjie Peng, Jin Wang, Yan Ling Cheah, Peifen Teh, Yahwen Ko, Chuiling Wong, and Madhavi Srinivasan. Facile Approach to Prepare Porous $CaSnO_3$ Nanotubes via a Single Spinneret Electrospinning Technique as Anodes for Lithium Ion Batteries. Acs Appl. Mater. Inter., 2012, 4(11): 6005
22. Y. L. Qin, F. F. Zhang, X. C. Du, G. Huang, Y. C. Liu, L. M. Wang. Controllable synthesis of cube-like $ZnSnO_3$@TiO_2 nanostructures as lithium ion battery anodes. J. Mater. Chem. A, 2015, 3(6): 2985-2990
23. J. F. Duan, S. C. Hou, S. G. Chen, H. G. Duan. Synthesis of amorphous $ZnSnO_3$ hollow nanoboxes and their lithium storage properties. Mater. Lett., 2014, 122: 261-264
24. Oiong Chen, Yuhua Wang, Mingxiao Wang, Shuyi Ma,Peiyu Wang, Guoheng Zhang, Wanjun Chen, Haiyan Jiao, Liwei Liu, Xiaoli Xu, Enhanced acetone sensor based on Au functionalized In-doped $ZnSnO_3$ nanofibers synthesized by electrospinning method. J. Colloid Interf. Sci., 2019, 543, 285-299
25. D. Lian. B. Shi, R. Dai. X. H. Jia, X. Y. Wu.Synthesis and enhanced acetone gas-sensing performance of $ZnSnO_3$/SnO_2 hollow urchin nanostructures, J. Nanopart. Res. 2017,19, 401.
26. J. Y. Liu,T. S. Wang, B. Q. Wang, P. Sun, Q. Y. Yang, X. S. Liang, H. W. Song, G. Y. Lu, Highly sensitive and low detection limit of ethanol gas sensor based on hollow ZnO/SnO_2 spheres composite material. Sensor. Actuat. B-Chem. 2017, 245, 551-559.
27. S. L. Bai, Y. Tian,Y. H. Zhao, H. Fu, P. G. Tang, R X. Luo, D. Q. Li, A F. Chen, C. C. Liu, Construction of NiO@$ZnSnO_3$ hierarchical microspheres decorated with NiO nanosheets for formaldehyde sensing, Sensor. Actuat. B-Chem. 2018, 259, 908-916.
28. M. A. Hashem, S. Akbar, P. Morris, Role of oxygen vacancies in nanostructured metal-oxide gas sensors:a review, Sensor. Actuat. B-Chem. 2019, 301,126845
29. Y. Zeng, Y. F. Bing, C. Liu, W. T. Zhang, G. T. Zou. Self-assembly of hierarchical $ZnSnO_3$-SnO_2 nanoflakes and their gas sensing properties. T. Nonferr. Metal. Soc., 2012, 22(10): 2451-2458
30. H. M. Gong, C. H. Zhao, G. Q. Niu, W. Zhang, F. Wang, Construction of 1D/2D α-Fe_2O_3/SnO_2 hybrid nanoarrays for sub-ppm acetone detection, Research 2020, 1, 304-314
31. L. Xiao, S. M. Shu, S. T. Liu, A facile synthesis of Pd-doped SnO_2 hollow microcubes with enhanced sensing performance, Sensor. Actuat. B-Chem. 2015, 221,120-126.